49th AIAA Aerospace Sciences Meeting including the New Horizons Forum and Aerospace Exposition
4 - 7 January 2011, Orlando, Florida

AIAA 2011-1036

Investigations of Peripheral 4-jet Sonic and Supersonic Propulsive Deceleration Jets on a Mars Science Laboratory Aeroshell

Joshua R. Codoni,[1] Erin M. Reed,[2] and James C. McDaniel[3]
Department of Mechanical and Aerospace Engineering, University of Virginia, Charlottesville, VA, 22903

Hicham Alkandry[4] and Iain D. Boyd[5]
Department of Aerospace Engineering, University of Michigan, Ann Arbor, MI, 48109

With the launch of Mars Science Laboratory (MSL), scheduled for 2011, Viking technology developed in the 1970's is reaching its limits for entry, descent and landing (EDL) on Mars, necessitating research and development of other technologies for decelerating high mass Mars entry systems (HMMES), such as propulsive deceleration (PD) jets. In this paper planar laser-induced iodine fluorescence is utilized to obtain qualitative flow visualization images and quantitative PD jet mole fraction images of peripheral sonic and supersonic PD jet models in Mach 12 flow and compared to CFD computations. The models are 0.22% of the MSL frontal area, with Mach 1 and Mach 2.66 jets on the frontal aeroshell of the model, oriented normal to the hypersonic flow. The interactions of PD jets with a Mach 12 freestream flow are visualized with coefficients of thrust (C_T) varying from 0.5 to 3.0 in increments of 0.5. It was found that as C_T increases the shock stand-off distance increases for both sonic and supersonic cases, with the supersonic distance at a C_T = 3.0 being 17% greater than the sonic distance. The jet penetration distance was measured to be 50% greater for the supersonic case at a C_T = 3.0. Experimental results were compared with CFD calculations of the sonic 4-jet configuration. Very good comparison was shown in the streamline patterns and jet mole fraction distributions. Using the validated CFD model, preliminary calculations showed that the drag coefficient for the 4-jet peripheral case was 3 times larger than that for the single centerline jet case at a C_T of 0.5 and 6 times larger at a C_T of 1.5, both with sonic exit conditions and the same total mass flow rate. The preservation of the vehicle drag was attributed to the normal bow shock between the peripheral jets which does not exist in the single centerline jet. The total axial force coefficient (sum of C_T and C_D) was calculated to be twice as large for the peripheral 4 sonic jets as for the single sonic centerline jet at a C_T of 0.5 and 50% larger at a C_T of 1.5. This result suggests that, for the same total mass flow rate and sonic exit Mach number, the propulsive deceleration performance of the peripheral 4-jet PD design will be considerably greater relative to the single centerline PD jet. This result is important for the design of PD jet decelerators for EDL for future HMMES missions.

Nomenclature

C_D	=	Coefficient of Drag
C_T	=	Thrust Coefficient
D	=	Diameter [m]
M	=	Mach Number
$\dot{m}$	=	Mass Flow Rate [kg/s]
p	=	Pressure [N/m^2]
q	=	Dynamic Pressure [N/m^2]
S	=	Aeroshell Frontal Area [m^2]
T	=	Thrust [N]
V	=	Velocity [m/s]
γ	=	Ratio of Specific Heats

[1] Graduate Student, Student Member AIAA.
[2] Graduate Student, Student Member AIAA.
[3] Professor, Associate Fellow AIAA.
[4] Graduate Student, Student Member AIAA.
[5] Professor, Associate Fellow AIAA.

Copyright © 2011 by the American Institute of Aeronautics and Astronautics, Inc. All rights reserved.

subscripts
e = Jet Exit Conditions
∞ = Freestream Conditions

I. Introduction

ENTRY, descent, and landing (EDL) is one of many challenging aspects of Mars missions. A thin atmospheric density, roughly 1% of Earth's, causes significant heating, but insufficient deceleration for high mass Mars entry systems (HMMES) [1]. Because of the thin atmosphere, as payload mass increases it becomes a greater challenge to adequately slow the landing vehicle quickly enough to facilitate parachute deployment and enter a landing configuration [1]. Therefore, as human-scale missions are planned – on the scale of orders of magnitude larger than landers to date – it becomes necessary to explore new methods for decelerating landing vehicles.

Retropropulsion, or propulsive deceleration (PD), has recently received renewed interest as an enabling technology for adequately decelerating HMMES at supersonic and hypersonic Mach numbers [2]. Single or multiple PD jets are fired from the aeroshell against the freestream velocity, using the jet thrust to achieve the deceleration. To date there is a dearth of experimental and computational data on multiple PD jets located around the periphery of the aeroshell [3]. The only available data conducted experiments for peripheral 3-jet PD models at freestream Mach numbers up to 6.0 using schlieren/shadowgraphs for visualizations and pressure taps/strain-gages for drag characteristics [4-6]. Previous experiments indicate that aerodynamic drag can be preserved to some extent while thrust force is increased for peripheral multiple jet configurations. Preservation of aerodynamic drag with increasing thrust shows promise for this technology as better enabling HMMES to decelerate. However little is known about the flow properties of the highly complex interaction of a supersonic/hypersonic freestream with sonic/supersonic peripheral PD jets.

This paper will present current work being performed at the University of Virginia to employ a technique known as planar laser-induced iodine fluorescence (PLIIF) to obtain visualization images for sonic and supersonic peripheral 4-jet PD models opposing a rarefied freestream at Mach 12. Experimental visualizations will be compared with computational fluid dynamic (CFD) numerical results obtained by the University of Michigan. Visualization images for multiple cases, as well as a quantitative PD jet mole fraction images, will be presented and discussed.

II. Experimental Technique (University of Virginia)

A. Facilities

PD jet experiments are conducted at the University of Virginia using a continuous flow hypersonic wind tunnel, as shown in Figure 1. The wind tunnel uses a continuously evacuated vacuum chamber to provide the low back pressures necessary to produce the hypersonic test section flow. Low chamber back pressures are achieved using three vacuum pumps – Stokes MicroVac pump, Roots Rotary Vane Booster pump, and a Roots Rotary Vane High Pressure pump – maintaining pressures on the order of 300 mtorr even when the main flow is introduced [7]. Three portholes in the wall of the vacuum chamber provide optical access for the collimated laser sheet necessary for PLIIF. A fourth porthole perpendicular to the laser sheet entry provides optical access for a CCD camera.

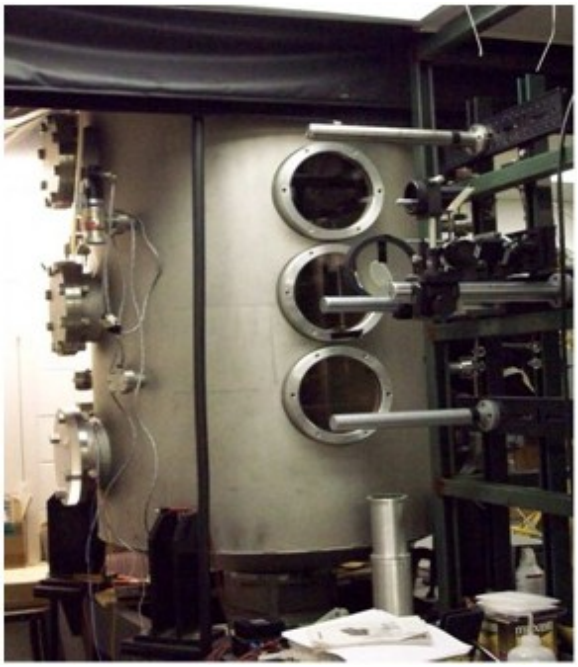

Figure 1: Hypersonic Wind Tunnel

The test section of the hypersonic wind tunnel is an underexpanded jet exhausting through a 2 mm sonic orifice into the continuously evacuated chamber [7]. As shown in Figure 2, the jet expands from a point source and produces a barrel shock, terminating in a Mach disk, approximately 8 cm downstream of the orifice. The isentropic core of the jet expansion provides a test section capable of Mach numbers from 1 to 16, and Knudsen numbers (ratio of mean free path to jet exit orifice diameter) to nearly 1. The Mach number, M, versus distance from the sonic orifice is calculated using the Ashkenas and Sherman relationship, as shown in equation 1:

$$M = A\left(\frac{x-x_0}{D}\right)^{\gamma-1} - \frac{1}{2}\left(\frac{\gamma+1}{\gamma-1}\right)\left[A\left(\frac{x-x_0}{D}\right)^{\gamma-1}\right]^{-1} \quad (1)$$

where x is the position along the jet centerline, and x_0 and A are constants empirically determined by Ashkenas and Sherman for the specific heat ratio corresponding to N_2, the test section gas [8]. MSL models are placed along the centerline of the underexpanded jet at positions corresponding to the desired Mach number calculated with the Ashkenas and Sherman relationship.

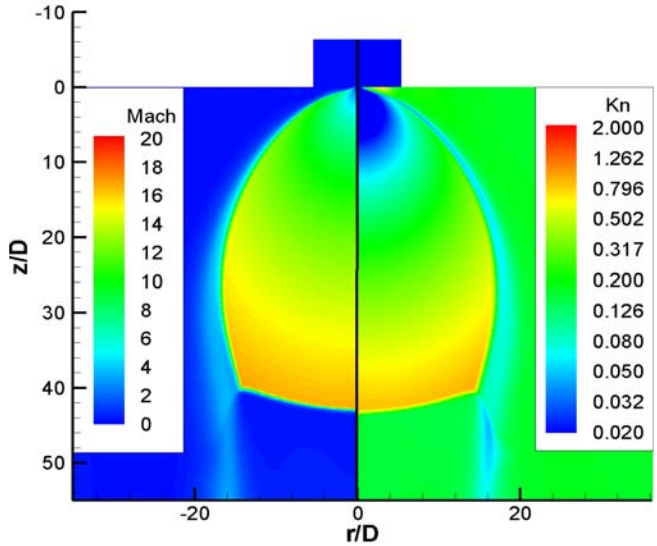

Figure 2: Calculation of model of Mach and Knudsen numbers in hypersonic test section [10]

B. PLIIF Experimental Method

PLIIF is an optical non-intrusive, time averaged measurement technique that has been extensively developed and used at the University of Virginia for nearly thirty years [7,9-12]. PLIIF uses I_2 as the fluorescing species and is capable of producing planar measurements for flow visualization, and quantitative measurement of mole fraction, velocity, pressure, density, and temperature. It is advantageous over other methods such as schlieren and shadowgraph due to its ability to provide sufficient signal for flowfield imaging even in rarefied regimes [10]. Another benefit of PLIIF is the ability to produce accurate measurements across shocks, unlike other methods such as particle image velocimetry [13].

The experimental set-up for the PLIIF method is pictured in Figure 3. A laser beam from a Spectra-Physics Beamlok 2080A argon ion laser, operating at 514.5 nm, is collimated into a thin laser sheet using a series of optics, pictured in the center right of Figure 1. The laser sheet propagates through the bottom porthole of the vacuum chamber and is incident on the top of the model after reflecting from two mirrors placed inside the chamber. The iodine fluoresces and this signal is captured at 90 degrees to the laser sheet by an Andor iKon-L CCD camera for exposure times from 10-45 seconds. Scattered laser light is blocked with a glass orange Heliopan #22 filter.

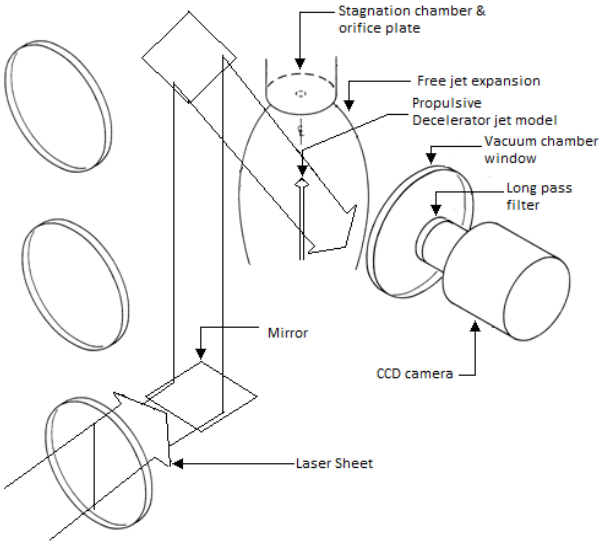

Figure 3: PLIIF Setup

C. Model Design

Visualization results for two models will be shown and discussed: a sonic peripheral 4-jet model and a supersonic peripheral 4-jet model. The models are 0.22% scale of the Mars Science Laboratory (MSL) frontal aeroshell. The jets for the sonic and supersonic models are oriented normal to the direction of freestream flow which causes the jet exit orifice to be slightly elliptical. The sonic jet model has a jet exit diameter of 0.5 mm while the supersonic jet model has a jet exit diameter of 0.9 mm, with a throat diameter of 0.5 mm, corresponding to a jet exit Mach number of 2.66. The models are constructed of 316 stainless steel and painted matte black to minimize scattered light reflections from inside the chamber. Nitrogen seeded with iodine is supplied to the PD jets via a sting mounted to the aft body of the model.

D. Thrust Calculations

In order to compare experimental data from other facilities and CFD results, a non-dimensional coefficient of thrust (C_T) is used. C_T, defined by McGhee as the ratio of jet thrust to the freestream dynamic pressure times the frontal area of the model is as follows [14]:

$$C_T = \frac{T}{q_\infty S} = \frac{\dot{m}V_e + (p_e - p_\infty)A_e}{q_\infty S} \tag{2}$$

The thrust coefficient in equation 2 was calculated using isentropic equations and the Ashkenas and Sherman (eq. 1) relationship for the freestream conditions.

III. CFD (University of Michigan)

Experimental results will be compared with numerical simulations from the University of Michigan. Numerical simulations are executed using LeMANS, a parallelized CFD code developed at the University of Michigan for simulating hypersonic reacting flows [15-18]. LeMANS solves the laminar three-dimensional Navier-Stokes equations on unstructured computational grids, including thermo-chemical nonequilibrium effects. Mixing transport properties can be calculated using several options. For this study mixing transport properties are calculated using Wilke's semi-empircal mixing with species viscosities calculated using Blottner's model and species thermal conductivities determined using Eucken's relation. The finite-volume method applied to unstructured grids is used to solve the set of partial differential equations. Time integration is performed using a point implicit or line implicit method [18].

The flow is modeled assuming that the continuum approximation is valid. Furthermore, for this work, it is assumed that the translational and rotational energy modes of all species can be described by two different temperatures T_{tra} and T_{rot}, respectively, while the vibrational energy mode and electron energy of all species are frozen at the stagnation value (i.e. 300 K). In order to accurately simulate the flow in the experimental facility, I_2-seeded N_2 gas is used in the numerical simulations with a seeding ratio of 200 ppm. In the freestream, the rotational temperature is assumed to be equal to the translational temperature. Also, the Ashkenas and Sherman boundary conditions are used as flow conditions input to LeMANS at the upstream boundary. The solution results in the flowfield shown in Figure 4 for a C_T of 0.5 and 1.5. The main flowfield features to be studied are demonstrated in Figure 4. The computation results in Figure 4 are for the sonic model with a C_T of 0.5 and 1.5. Freestream flow is from left to right, the bow shock, PD jet flow structure and PD shock are as indicated.

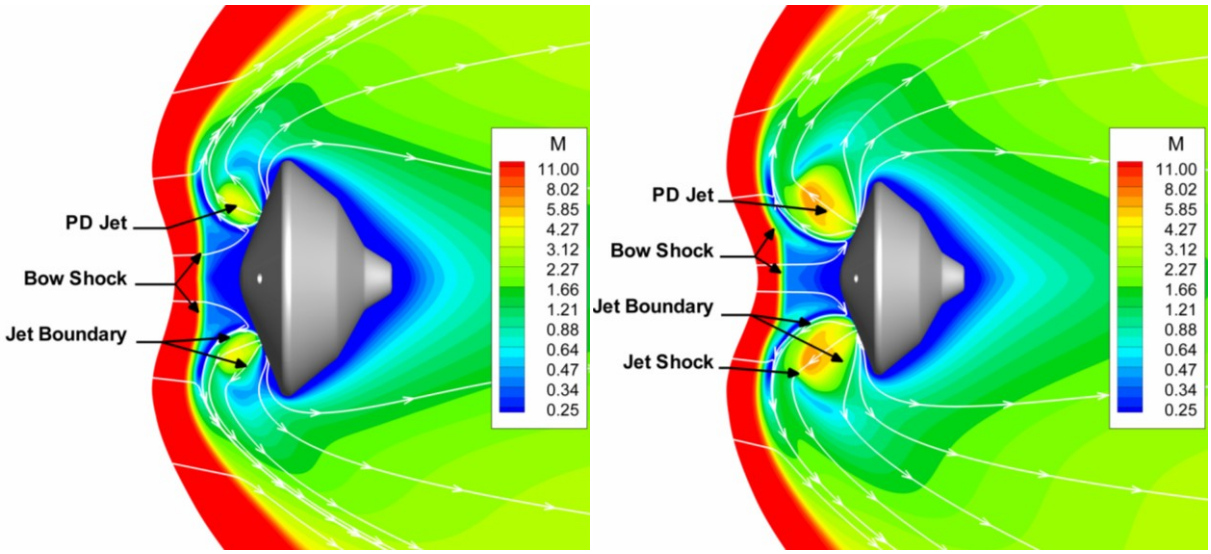

(a) $C_T = 0.5$ (b) $C_T = 1.5$

Figure 4: CFD computation of sonic 4-jet PD model, log scale

IV. Results

A. Experimental Visualizations

Figures 5 and 6 are experimental PLIIF visualizations of the sonic and supersonic peripheral 4-jet PD models, respectively, at C_T from 0.5 to 3.0 in increments of 0.5. Freestream flow is from the top of the images to the bottom. The forebody of the model MSL aeroshell is placed at the Mach 12 location in the hypersonic underexpanded jet test flowfield. The model is superimposed in the images to better orient the reader with the geometry of the image. In these images only two of the four jets are visible since the laser sheet passes through the center of two jets only. Furthermore, the flowfields are symmetric, so the images are mirrored about the model centerline to remove the Doppler shift effect which is otherwise observed in the fluorescence images [12].

The sonic PD jets (Figure 5) are underexpanded jets much like the hypersonic test flowfield. The PD jets exit the orifice at Mach 1 and freely expand until they terminate in the jet shock. The PD jets cause the MSL bow shock to be pushed away from the model forebody. The bow shock location above the centerline of the model between the jets increases from a location which is approximately 15% of the frontal model diameter at a C_T of 0.5 to roughly 50% at a C_T of 3.0. The significance of this bow shock will be discussed later. For smaller C_T values, 0.5 to 1.5, there is fluorescence around the shoulder of the model from the aeroshell forebody which is not present at larger C_T values.

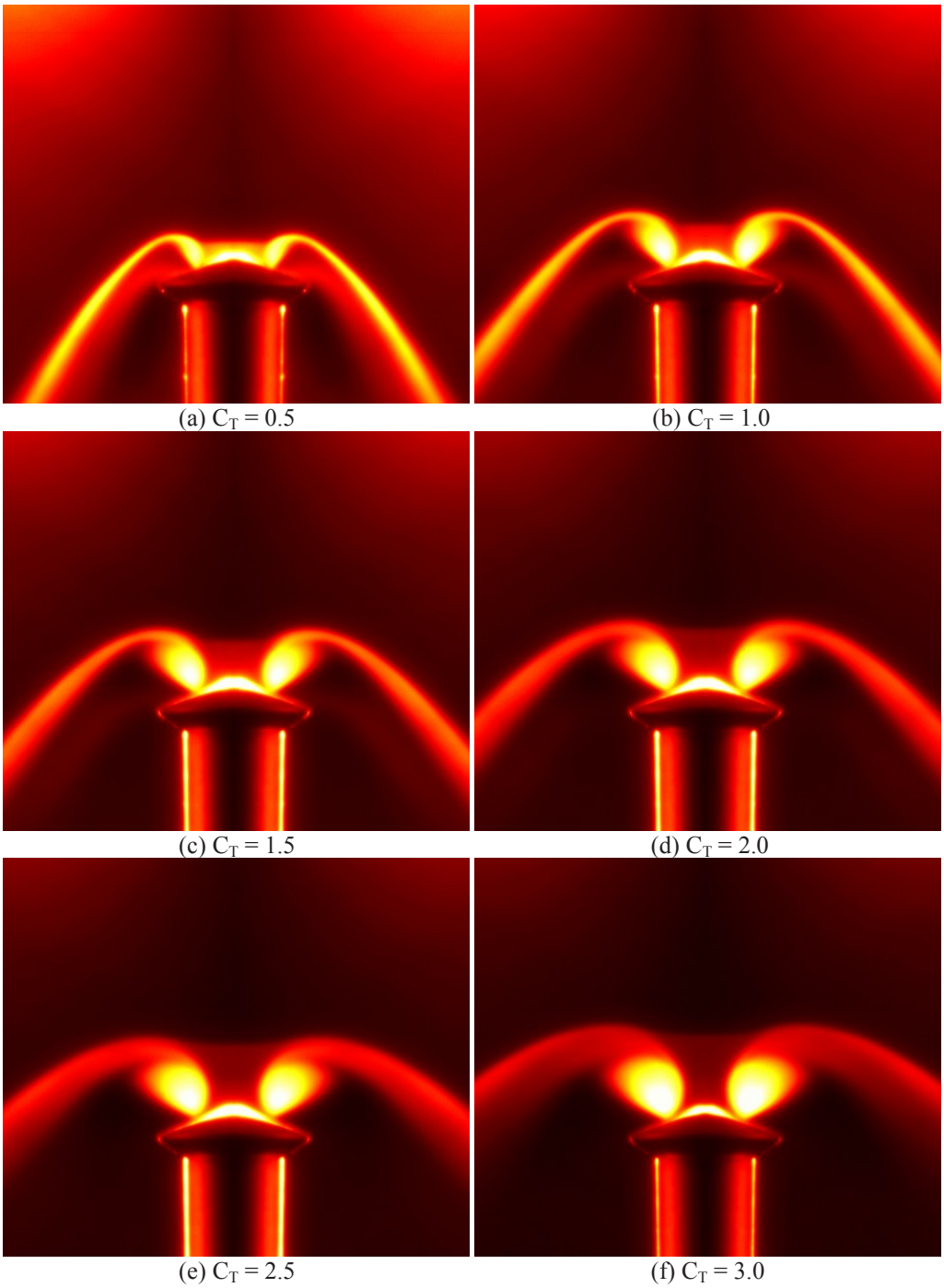

(a) $C_T = 0.5$ (b) $C_T = 1.0$

(c) $C_T = 1.5$ (d) $C_T = 2.0$

(e) $C_T = 2.5$ (f) $C_T = 3.0$

Figure 5: Sonic peripheral 4-jet PD model, $M_{jet} = 1.0$, for range of C_T from 0.5 (a) to 3.0 (f).

Figure 6 is the supersonic peripheral 4-jet PD model and has a jet exit Mach number of 2.66, based on the nozzle area ratio. It is seen that the supersonic PD jets push up the bow shock further from the aeroshell than the sonic jets. The sonic PD jets have a larger jet turning angle than the supersonic case and a jet boundary that is broader. The shock stand-off distance, SSD, directly above the model centerline, normalized to the model frontal diameter, is shown in Figure 7 versus C_T. The stand-off distance for the supersonic case is approximately the same as the sonic case until a C_T of 1.5. For C_T of 3.0 the shock stand-off distance is about 17% greater for the supersonic case. Like the sonic case, the supersonic case also has fluorescence around the shoulder of the model for small values of C_T. The non-distinct boundaries of the shock above the supersonic jets for a C_T of 3.0 could indicate unsteady flow.

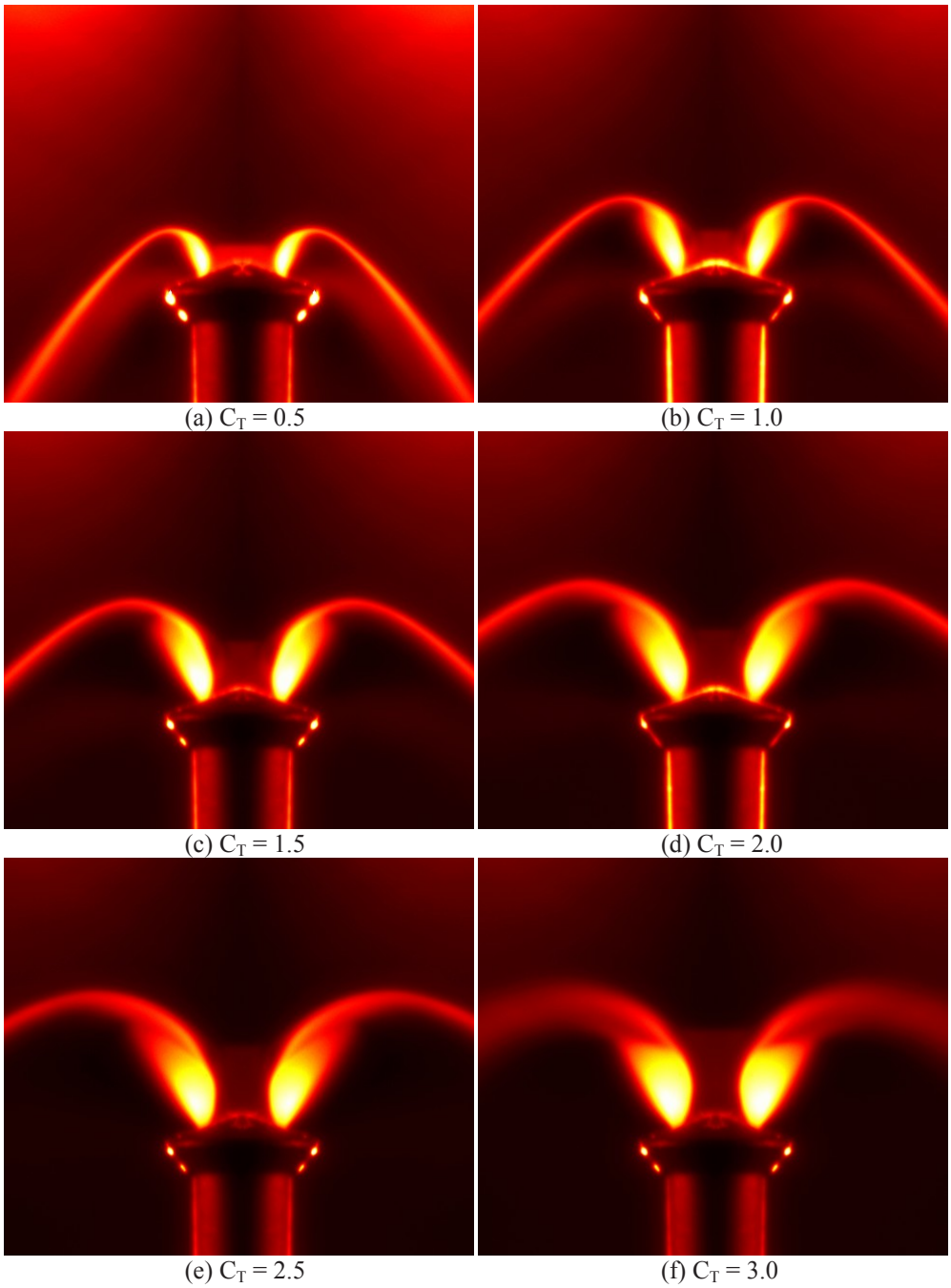

(a) $C_T = 0.5$ (b) $C_T = 1.0$

(c) $C_T = 1.5$ (d) $C_T = 2.0$

(e) $C_T = 2.5$ (f) $C_T = 3.0$

Figure 6: Supersonic periphery 4-jet PD model, $M_{jet} = 2.66$, for C_T from 0.5 (a) to 3.0 (f).

The maximum PD jet penetration distance, normalized to the model aeroshell diameter, versus C_T, is shown in Figure 8. The graph reflects the trends seen in the images: the supersonic jets extend further into the freestream than the sonic jets for all C_T tested, even for small C_T where the shock stand-off is roughly the same. The penetration distance for the supersonic case is 50% greater than the sonic case at $C_T = 3.0$.

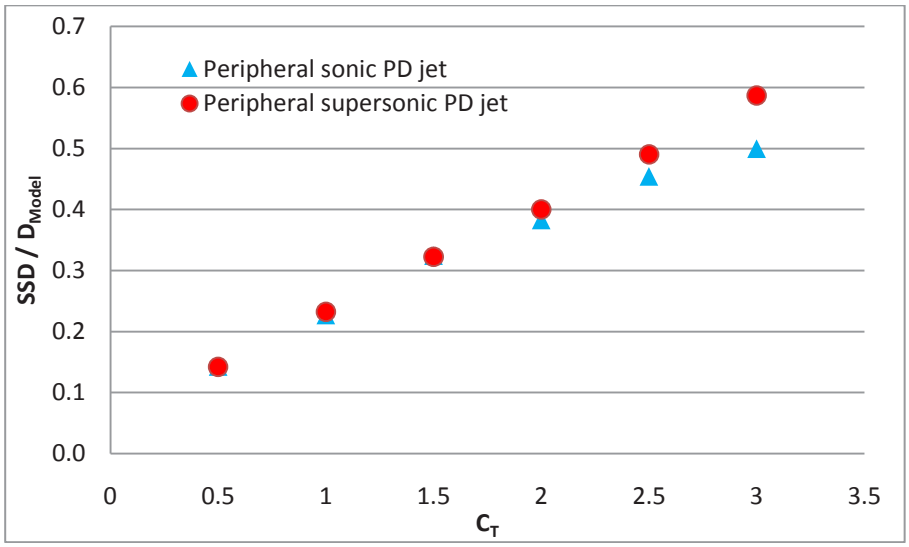

Figure 7: Shock stand-off comparison of sonic and supersonic PD models

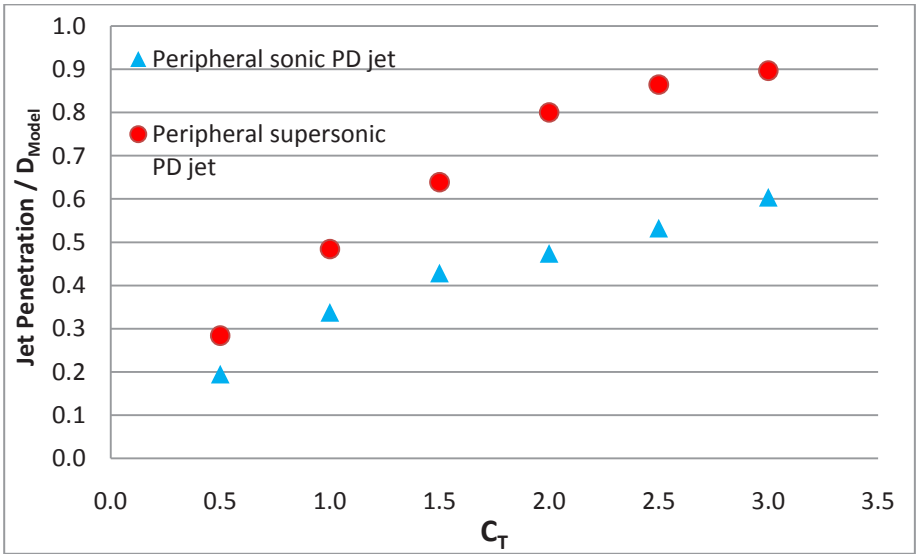

Figure 8: Jet penetration comparison of sonic and supersonic PD models

Quantitative mole fraction images were also obtained using PLIIF. By taking the ratio of a jet-only seeded image to a full flow seeded image (Figure 9(a) divided by 9(b)) and normalizing the ratio by the value in the PD core where the jet mole fraction is unity, a jet mole fraction image results [19]. The fluorescence above the center of the model, between the PD jets, is only visible in the full flow seeded case (Figure 9(b)) which indicates the fluid in this region of the image is solely from compressed fluid behind the bow shock from the freestream flow. The significance of the bow shock seen in Figure 9(b) will be discussed later. The results of the mole fraction images are shown in Figure 10 for the sonic and supersonic PD jet models for a C_T of 1.5. The color contours give spatially-resolved quantitative values of the local jet mole fraction which are due to the PD jet mixing with the Mach 12 freestream. These quantitative images provide the opportunity to validate CFD results, as will be shown in the next section of this paper.

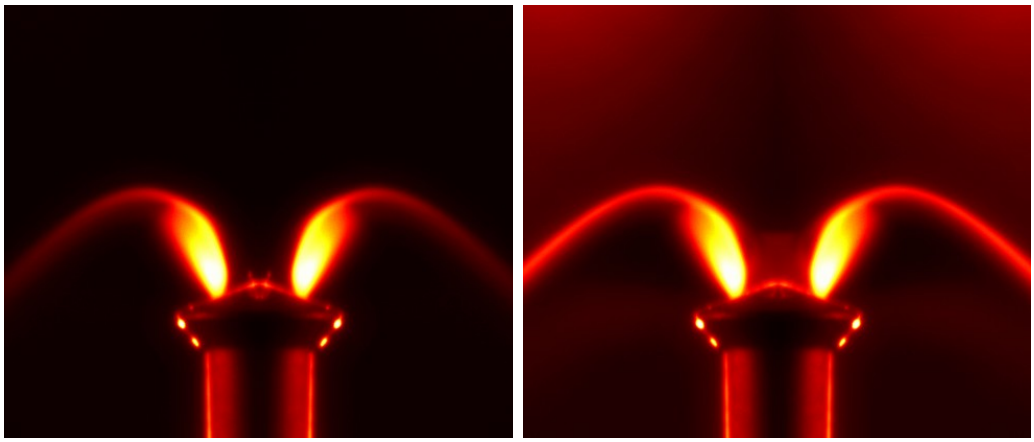

(a) C_T = 1.5, jet only seeded (b) C_T = 1.5, full flow seeded

Figure 9: Supersonic peripheral 4-jet PD model, M_{jet} = 2.66, for two iodine seeding cases

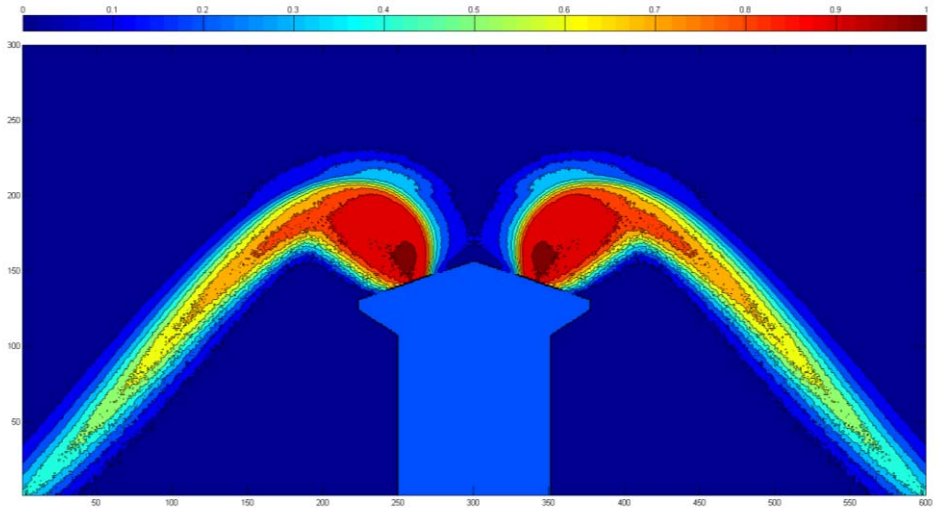

(a) Sonic peripheral 4-jet PD model, M_{jet} = 1.0

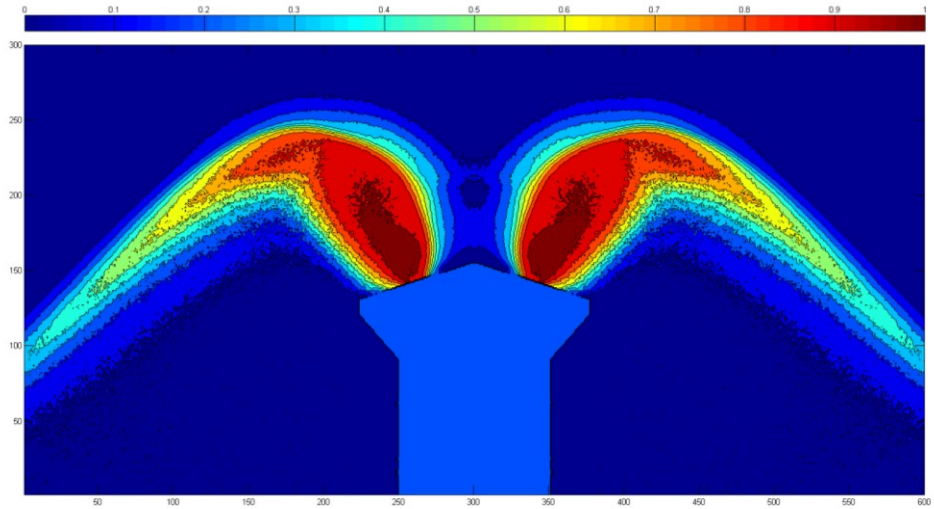

(b) Supersonic peripheral 4-jet PD model, M_{jet} = 2.66

Figure 10: Experimental 4-jet PD mole fraction images, C_T = 1.5

B. Numerical Simulation Comparisons

CFD calculated streamlines overlay the experimental visualizations of the sonic model for C_T of 0.5 and 1.5 in Figure 11. Overall there is very good agreement between the CFD calculated streamlines and the shock structure and jet mixing as seen in the visualizations. The CFD calculations begin in the PD jet plenum and calculate the flow through the jet nozzle. It is seen that the PD jet freely expands from the nozzle exit until the bow shock, at which point the flow is swept out away from the model and downstream. Between the PD jets the freestream flow compresses in a shock and the streamlines continue down to the model surface, at which point they reverse direction and follow the PD jet flow out from the model and downstream.

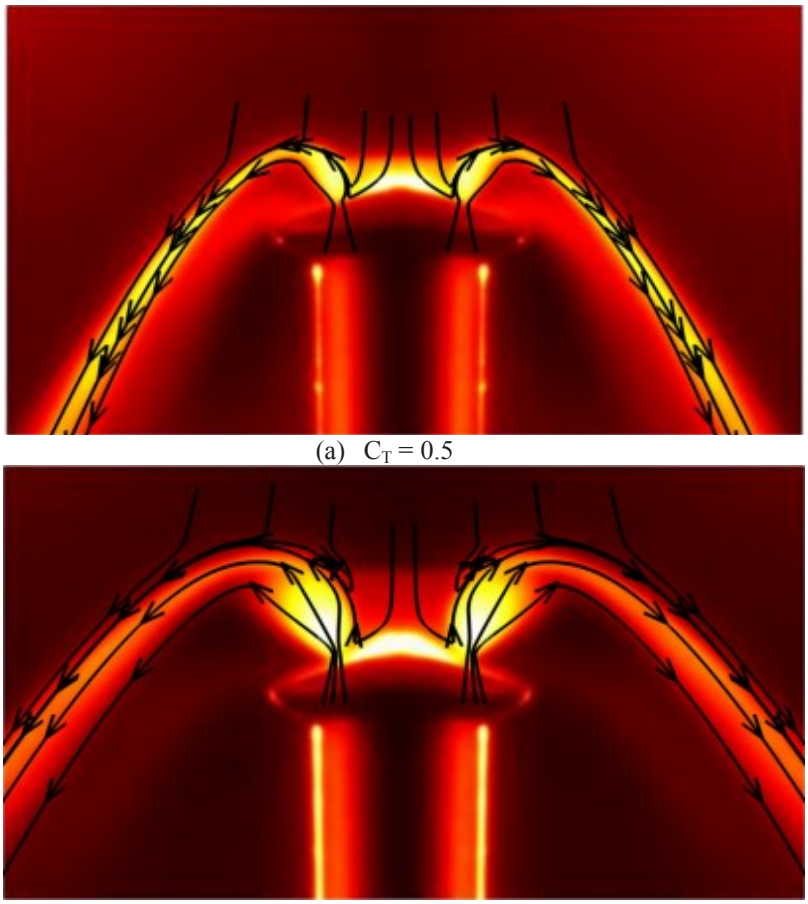

(a) $C_T = 0.5$

(b) $C_T = 1.5$

Figure 11: Numerical calculation of streamlines with experimental visualization, sonic PD model $M_{jet} = 1.0$

Comparisons between CFD and experimental mole fraction for the sonic model are shown in Figure 12 for a C_T of 1.5. Overall there is good agreement between the CFD calculations and the quantitative experimental results. Discrepancies arise after the shoulder of the model in part due to two factors. First, physical constrains limit the experimental aft body model angle to 35 degrees whereas the CFD utilizes a model with a 50 degree aft body angle. Secondly, CFD does not yet take into account the model sting. Both of these factors could contribute to the greater expansion that is observed in the CFD relative to the experiment downstream of the model shoulder; however since the pressure is very low on the vehicle aft body, it is expected that this discrepancy will not have a significant impact on the calculation of the vehicle drag coefficient. Experimental results do not resolve any jet fluid mixing downstream of the model near the sting. Figure 13 plots the jet mole fraction versus the distance L, normalized by the model diameter D, for the CFD calculations and PLIIF results along the lines A and B as seen in Figure 12. Profile A, through the jet core, corresponds to the nozzle exit at $L/D_{model} = 0$ and increases away from the nozzle exit.The sharp drop in jet mole fraction across the jet boundary and shock is clearly visible. Profile B, a cross sectional cut in the jet core, is centered at $L/D_{model} = 0$ which corresponds to the intersection of lines A and B in Figure 12. L/D_{model} increasing indicates moving toward the shoulder of the model, as shown in Figure 12. Once

again the jet mole fraction drops off sharply across the jet boundaries. Very good agreement is seen between the quantitative PLIIF mole fraction profiles and the CFD predictions.

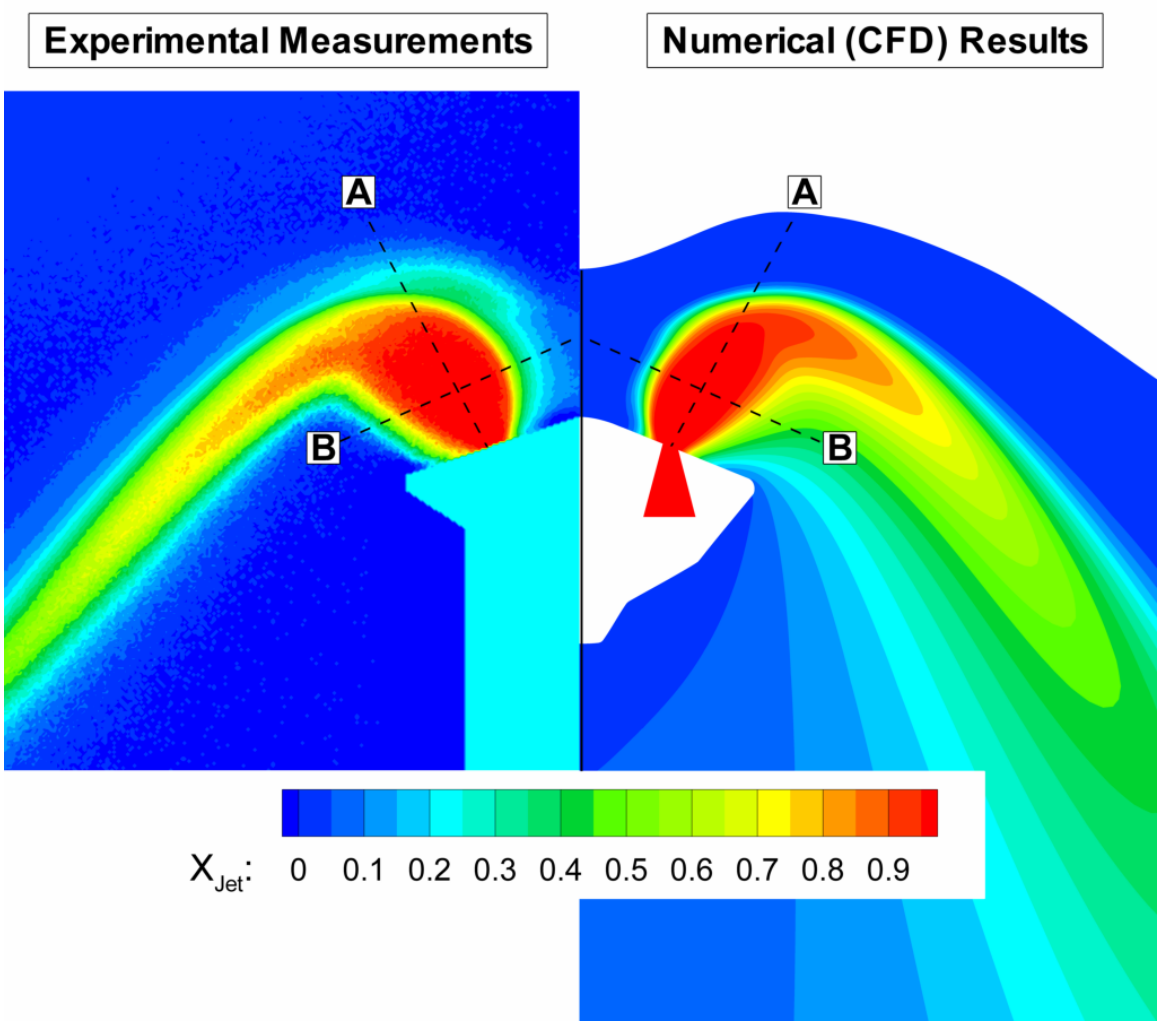

Figure 12: Experimental PD jet mole fraction compared to CFD, sonic model, $M_{jet} = 1.0$, $C_T = 1.5$

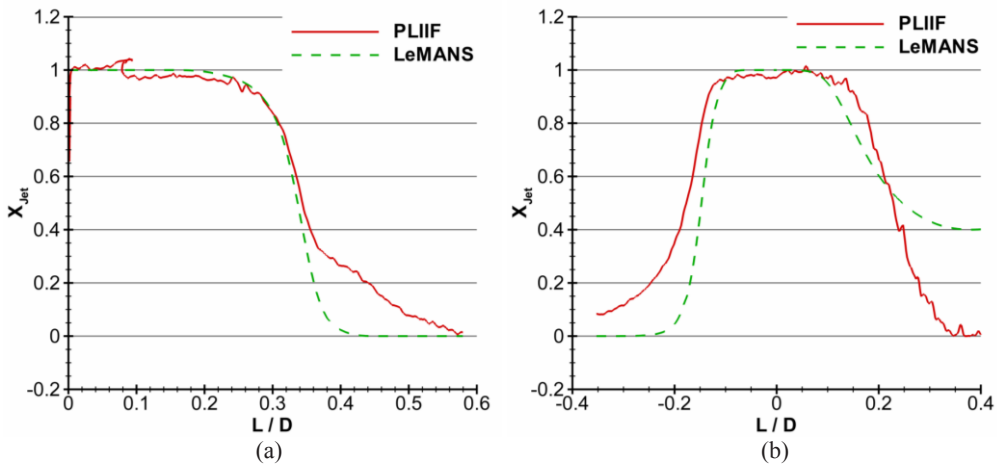

Figure 13: Experiment jet mole fraction and CFD comparison along lines A and B in Figure 12

Calculated coefficient of drag (C_D) and total axial force (sum of C_D and C_T) for the sonic peripheral 4-jet configuration and sonic single centerline (Central) jet configuration are shown in Figure 14. As shown in this figure, C_D decreases when the peripheral jets are turned on for C_T = 0.5 and 1.5; however, the decrease is considerably less than the previous reported [18] single centerline jet case also shown in this figure. The total axial force in the 4-jet peripheral case increases, even for C_T = 0.5, unlike the single centerline (Central) sonic case, which can be seen to decrease for low C_T. The C_D is approximately 3 times greater for the peripheral case than for the single centerline case for a C_T of 0.5 and 6 times greater for a C_T of 1.5. The total axial force coefficient is 2 times greater for the peripheral case at a C_T of 0.5 and 1.5 times greater at a C_T of 1.5. This implies that the propulsive deceleration with 4 peripheral jets will be twice that of a single centerline jet (both with sonic orifices and the same total mass flow rate) for a C_T = 0.5 and 50% greater for C_T = 1.5. It is likely that this vehicle drag preservation by the peripheral jets is caused by the presence of the normal bow shock between the jets (as seen in Figures 4, 5, 6, 9(b) and 11), unlike the single centerline jet which reduces the strength of the vehicle bow shock wave.

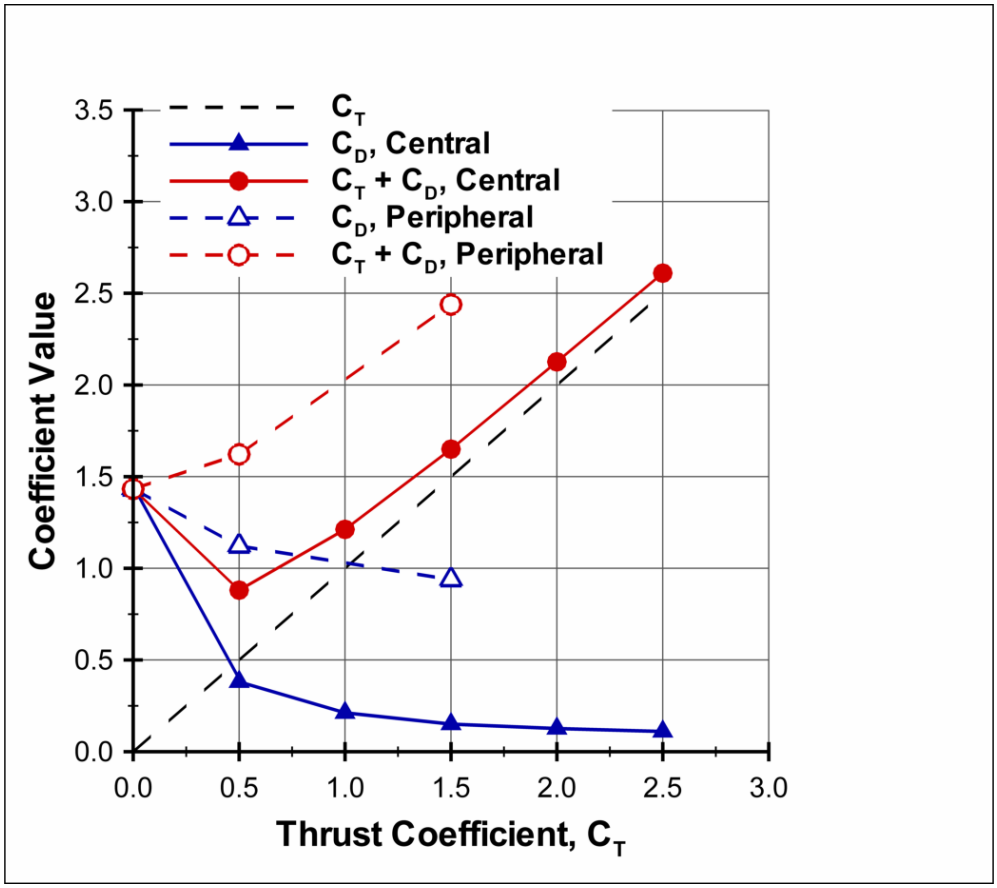

Figure 14: Drag and total axial force coefficients for sonic centerline (Central) and sonic 4-jet peripheral (Peripheral) models

V. Conclusion

Experimental qualitative PLIIF flow visualizations and quantitative mole fraction images have been presented and discussed for multiple sonic and supersonic peripheral jets on a MSL frontal aeroshell at Mach 12. Experimental results for the range of C_T from 0.5 to 3.0, in increments of 0.5, have demonstrated that as C_T increases shock stand-off distance also increases, with a 17% greater value for the supersonic jets relative to the sonic 4-jet PD model at a C_T of 3.0. The jet penetration for the supersonic case was measured to be approximately 50% greater than the sonic case at a C_T of 3.0. Further differences in the flow fields were observed, including a greater PD jet turning angle and broader jet boundary in the sonic case and possible flow unsteadiness in the supersonic case at the highest C_T, as demonstrated by the non-distinct bow shock structure in the image.

CFD appears to capture the major flow characteristics as shown by the experimental results. Overall there is good agreement between shock structure and calculated CFD streamlines for the sonic PD model at C_T of 0.5 and 1.5.

Mole fraction calculations are in good agreement with the experimental results, however there is some difference around the model shoulder, where CFD predicts more flow expansion. This difference could be due to the slightly different aft body angle of the experimental model and influence of the mounting sting.

Using the validated CFD model, preliminary calculations have shown that for the peripheral jet case versus the centerline jet case (both with sonic exit flow and same total mass flow rate), the peripheral 4-jet case versus the single centerline has 3 times greater C_D at $C_T = 0.5$ and 6 times greater at $C_T = 1.5$. This is likely due to the normal bow shock that exists between the peripheral jets which preserves the vehicle drag relative to the single centerline jet case which weakens the vehicle bow shock. The total axial force coefficient (sum of C_D and C_T) was calculated to be 2 times greater for the peripheral jets for $C_T = 0.5$ and 50% greater for $C_T = 1.5$. This implies that the propulsive deceleration with 4 peripheral jets will be significantly greater than that with a single centerline jet. This result is important to the design of PD jet systems for EDL for future HMMES missions.

VI. Future Work

Future CFD work will include calculations with the same physical model geometry as the experiment, as well as an inclusion of the model sting in these calculations. The CFD calculations will also be done for $C_T = 1.0$, 2.0, and 2.5 in order to more completely characterize the results shown in Figure 14 above. Future experimental work will produce quantitative measurements of flowfield temperature, pressure, density and velocity for selected C_T values at the University of Virginia. These additional quantitative results will again be compared with computed results from the University of Michigan.

Acknowledgments

This work is supported by Virginia Space Grant Consortium Fellowships (Codoni and Reed) and NASA Hypersonics Project NRA Grant NNX08AH37A, with Bryan Palaszewski from the NASA Glenn Research Center as the technical monitor. The University of Michigan would like to acknowledge the use of supercomputers in their Center for Advanced Computing and in the NASA Advanced Supercomputing Division.

References

1. Braun, R.D. and Manning, R.M., "Mars Exploration Entry, Descent, and Landing Challenges," Journal of Spacecraft and Rockets, Vol. 44, No. 2, pp. 310-323, March – April 2007.

2. Dwyer-Cianciolo, A.M., Davis, J.L., Komar, D.R., Munk, M.M., Samareh, J.A., Powell, R.W., Shidner, J.D., Stanley, D.O., Wilhite, A.W., Kinney, D.J., McGuire, M.K., Arnold, J.O., Howard, A.R., Sostaric, R.R., Studak, J.W., Zumwalt, C.H., Llama, E.G., Casoliva, J., Ivanov, M.C., Clark, I., and Sengupta, A., "Entry, Descent and Landing Systems Analysis Study: Phase 1 Report," NASA TM-2010-0000002009, July 2010.

3. Korzun, A.M., Braun, R.D. and Cruz, J.R., "Suvery of Supersonic Retropropulsion Technology for Mars Entry, Descent, and Landing," Journal of Spacecraft and Rockets, Vol. 46, No. 5, September-October 2009.

4. Jarvinen, P.O and Adams, R.H., "The Aerodynamic Characteristics of Large Angled Cones with Retrorockets," NASA Contract No. NAS 7-576, February 1970.

5. Jarvinen, P.O. and Adams, R.H., "The Effects of Retrorockets on the Aerodynamic Characteristics of Conical Aeroshell Planetary Entry Vehicles," AIAA Paper 70-219, January 1970.

6. Keyes, J.W. and Hefner, J.N., "Effect of Forward-Facing Jets on Aerodynamic Characteristics of Blunt Configurations at Mach 6," Journal of Spacecraft and Rockets, Vol. 4, No. 4, 1967, pp. 533-534.

7. Cecil, D.E., Planar Laser-Induced Iodine Fluorescence Measurements in Rarefied Hypersonic Flow Over a Reaction Control Jet Model in a Free Jet Wind Tunnel. M.S. Thesis, University of Virginia, January 2004.

8. Ashkenas, H. and Sherman, F.S., "The Structure and Utilization of Suerpsonic Free Jets in Low Density Wind Tunnels," Rarefied Gas Dynamics, Vol. 2, Academic Press, New York, 1966.

9. Cecil, D.E. and McDaniel, J.C., "Planar Laser-Induced Iodine Fluorescence Measurements in Rarefied Hypersonic Flow," Rarefied Gas Dynamics: 24th International Symposium, American Institute of Physics, 2005, Toronto, Canada, pp. 1325-1350.

10. Staack, D., McDaniel, J.C., Glass C.E., and Miller C., "Experimental Study of Interacting Rarefied and Continuum Flows." AIAA Paper 2001-2762, June 2001.

11. Hartfield, R.J., Hollo, S.D., and McDaniel, J.C., "Planar Temperature Measurement in Compressible Flows Using Laser-Induced Iodine Fluorescence," Optics Letters, Vol. 16, No. 2, 1991.

12. Reed, R., Codoni J., McDaniel, J.C., Alkandry, H., Boyd, I.D., "Investigation of the Interactions of Reaction Control Systems with Mars Science Laboratory Aeroshell," AIAA Paper 2010-1558, January 2010.

13. Hiller, B., Combined Planar Measurments of Velocity and Pressure Fields in Compressible Gas Flows Using Laser-Induced Iodine Fluorescence. Ph.D. dissertation, Stanford, Nov. 1986.

14. McGhee, R.J., "Effects of a Retronozzle Located at the Apex of a 140° Blunt Cone at Mach Numbers of 3.00, 4.50, and 6.00," NASA TN D-6002, January, 1971.

15. Scalabrin, L.C. and Boyd, I.D., "Development of an Unstructured Navier-Stokes Solver for Hypersonic Nonequilibrium Aerothermodynamics," AIAA Paper 2005-5203, June 2005.

16. Scalabrin, L.C. and Boyd, I.D., "Numerical Simulation of Weakly Ionized Hypersonic Flow for Reentry Configurations," AIAA Paper 2006-3773, June 2006.

17. Scalabrin, L.C. and Boyd, I.D., "Numerical Simulations of the FIRE-II Convective and Radiative Heating Rates," AIAA Paper 2007-4044, June 2007.

18. Alkandry, H., Boyd, I.D., Reed, E.M., Codoni, J.R., and McDaniel, J.C., "Interactions of Single-Nozzle Sonic Propulsive Deceleration Jets on Mars Entry Aeroshells," AIAA Paper 2010-4888, June 2010.

19. Hartfield, R.J., Abbitt, J.D., and McDaniel, J.C., "Injectant mole-fraction imaging in compressible mixing flows using planar laser-induced iodine fluorescence," Applied Optics, Vol. 14, No. 16, 1989.